

# Discotic liquid crystals of transition metal complexes, 31:† establishment of mesomorphism and thermochromism of bis[1,2- bis(4-*n*-alkoxyphenyl)ethane-1,2-dithiolene]nickel complexes‡

Hiroko Horie, Akira Takagi, Hiroshi Hasebe, Takumi Ozawa and Kazuchika Ohta\*

Department of Functional Polymer Science, Faculty of Textile Science and Technology, Shinshu University, 386-8567 Ueda, Japan. E-mail: ko52517@giptc.shinshu-u.ac.jp

Received 4th September 2000, Accepted 9th January 2001

First published as an Advance Article on the web 12th February 2001

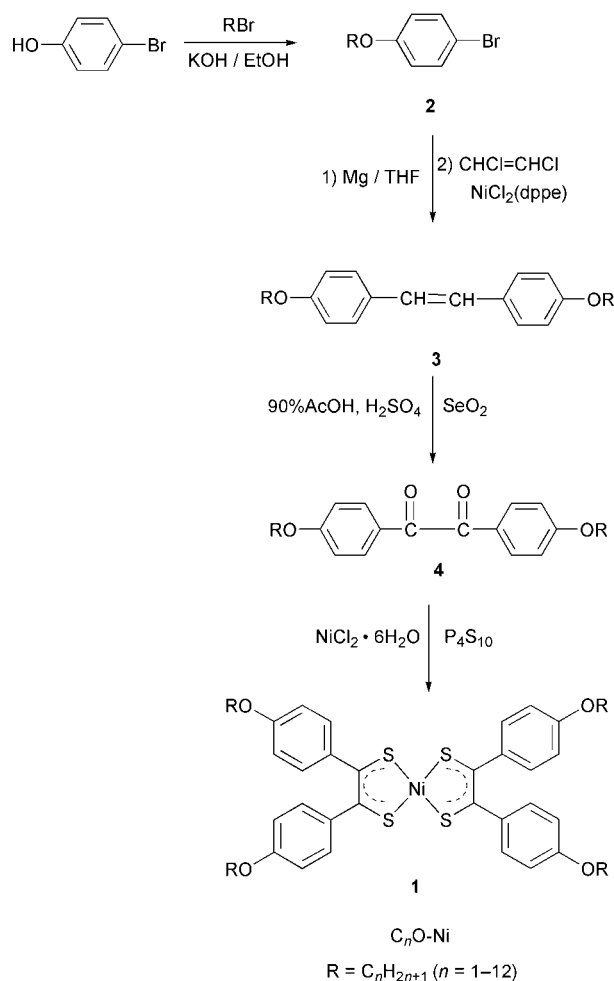
Two series of bis[1,2-bis(4-*n*-alkylphenyl)ethane-1,2-dithiolene]nickel,  $C_n$ -Ni ( $n=1-12$ ), and bis[1,2-bis(4-*n*-alkoxyphenyl)ethane-1,2-dithiolene]nickel,  $C_nO$ -Ni ( $n=1-12, 14, 16, 18$ ), have been synthesized. Their mesomorphism, thermochromism, supramolecular structures and  $\pi$ -acceptor property have been investigated by using different scanning calorimetry, polarizing microscopy, temperature-dependent X-ray diffraction technique, electronic spectroscopy and cyclic voltammetry. From the X-ray diffraction and electronic spectral results, it was established that the  $C_nO$ -Ni complexes for  $n \leq 10$  exhibit two differently colored discotic lamellar ( $D_L$ ) mesophases whereas none of the  $C_n$ -Ni complexes has a mesophase, and that the thermochromism (brown  $\rightarrow$  green) is attributable to a slow transformation from the Ni-Ni bonded dimers to the Ni-S bonded dimers.

## 1. Introduction

In 1977, the first calamitic liquid crystalline dithiolene metal complex was reported by Giroud and Mueller-Westerhoff.<sup>2,3</sup> Since then, **two** long chain-substituted rod-like dithiolene transition metal (Ni, Pt) complexes which show smectic and nematic liquid crystal phases have been studied.<sup>3-7</sup> These dithiolene metal complexes have unusual electronic structures to make them superior electron acceptors.<sup>3,5-7</sup>

In 1983, it was reported by Veber *et al.* that **four** long chain-substituted dithiolene nickel complex bis[1,2-bis(4-*n*-dodecyloxyphenyl)ethane-1,2-dithiolene]nickel (abbreviated as  $C_{12}O$ -Ni) shows a mesophase.<sup>8</sup> In 1986, we also synthesized the homologous complexes ( $n=9, 11$ ), using a different synthetic route (Scheme 1) and reported that these complexes exhibit a discotic mesophase.<sup>9,10</sup> However, in 1987, Veber *et al.* denied the existence of mesomorphism in these four long chain-substituted complexes and they claimed that the phase is not mesomorphic but crystalline.<sup>11</sup> Prior to this paper, Takagi in our group had already synthesized a series of the homologous  $C_nO$ -Ni and  $C_n$ -Ni complexes for  $n=1-12$ , using synthetic routes illustrated in Schemes 1 and 2. He found a mesophase in  $C_nO$ -Ni for  $n=9, 11$ , two mesophases in  $C_nO$ -Ni for  $n=10, 12$ , and no mesophase in all the  $C_n$ -Ni complexes.<sup>12</sup> He also noticed two differently colored mesophases for  $C_{12}O$ -Ni that Veber *et al.* had overlooked.

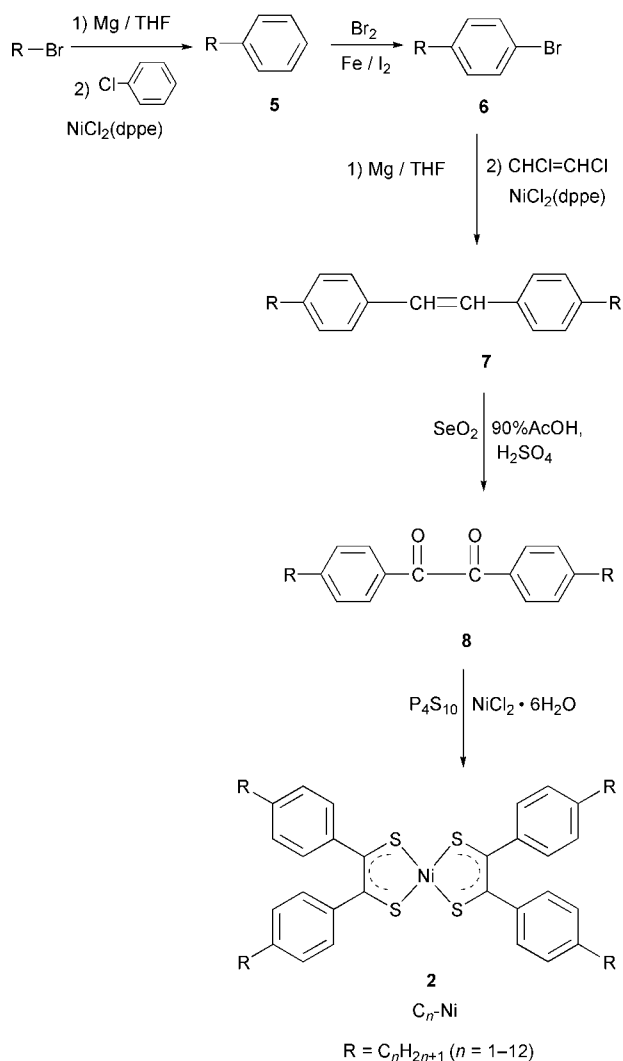
Hence, in order to establish the mesomorphism and thermochromism of  $C_nO$ -Ni, we have synthesized additional  $C_nO$ -Ni homologues for  $n=14, 16, 18$  by a novel synthetic route (Scheme 3) different from the previous two routes, and reinvestigated the physical properties in detail for all the complexes,  $C_nO$ -Ni ( $n=1-12, 14, 16, 18$ ) and  $C_n$ -Ni ( $n=1-12$ ).



**Scheme 1** Previous synthetic route for bis[1,2-bis(4-*n*-alkoxyphenyl)ethane-1,2-dithiolene]nickel, **1**. EtOH = ethanol, THF = tetrahydrofuran,  $NiCl_2(dppe)$  = dichloro[1,3-bis(diphenylphosphino)ethane]nickel(*n*), and AcOH = acetic acid.

†For part 30, see ref. 1.

‡Elemental analysis data and yields for compounds  $C_n$ -Ni and  $C_nO$ -Ni are available as supplementary data. For direct electronic access see <http://www.rsc.org/suppdata/jm/b0/b007135h/>

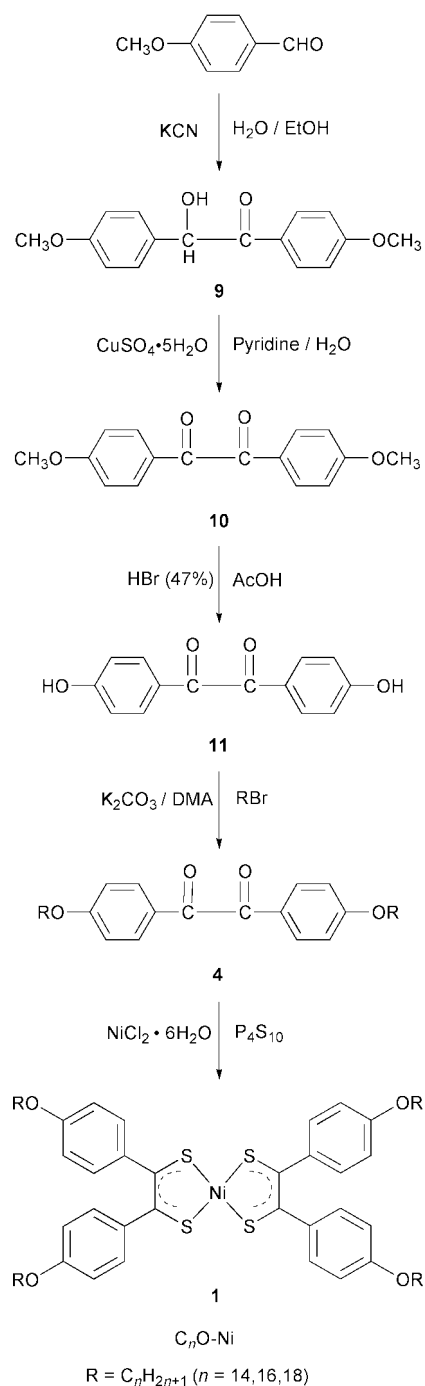


**Scheme 2** Synthetic route for bis[1,2-bis(4-*n*-alkylphenyl)ethane-1,2-dithiolene]nickel, **2**. EtOH = ethanol, THF = tetrahydrofuran, NiCl<sub>2</sub>(dppe) = dichloro[1,3-bis(diphenylphosphino)ethane]nickel(II), and AcOH = acetic acid.

## 2. Experimental

### 2.1 Synthesis

**Synthesis A.** The synthetic route to the C<sub>*n*</sub>O–Ni complexes for *n* = 1–12 is shown in Scheme 1.<sup>9,10,12</sup> In this synthetic route 4-bromophenol, the starting material, was converted to 4-*n*-alkoxybromobenzene **2**. The reaction of the Grignard reagent prepared from 4-*n*-alkoxybromobenzene with (*Z*)-dichloroethylene in the presence of dichloro[1,3-bis(diphenylphosphino)propane]nickel(II) gave 4,4'-di-*n*-alkoxystilbene **3** (Tamao–Kumada reaction<sup>13</sup>). 4,4'-Di-*n*-alkoxybenzil **4** was obtained by oxidation of the stilbene derivative **3** by selenium dioxide.<sup>14</sup> The preparation of the ligand and the formation of the complex was carried out in one pot; 4,4'-di-*n*-alkoxybenzil **4** was treated with phosphorus pentasulfide and then the complexation was carried out *in situ* with nickel chloride hexahydrate. All the 4,4'-di-*n*-alkoxybenzil **4** and the corresponding C<sub>*n*</sub>O–Ni complexes **1** were recrystallized from *n*-hexane and ethyl acetate, respectively. These C<sub>*n*</sub>O–Ni complexes recrystallized from ethyl acetate are black for *n* = 1–5, dark brown for *n* = 6 and brown for *n* = 7–18, as summarized in



**Scheme 3** New synthetic route for bis[1,2-bis(4-*n*-alkoxyphenyl)ethane-1,2-dithiolene]nickel, **1**. AcOH = acetic acid, DMA = *N,N*-dimethylacetamide.

Table 1. In the electronic supplementary data,<sup>†</sup> the elemental analysis data, yields and the crystalline shapes obtained from recrystallization are summarized. The detailed procedures were described in a previous paper.<sup>10</sup>

**Synthesis B.** The synthetic route to the C<sub>*n*</sub>–Ni complexes for *n* = 1–12 is shown in Scheme 2. The alkyl-substituted nickel complexes, C<sub>*n*</sub>–Ni (**2**; *n* = 1–12), could be prepared by almost the same synthetic route illustrated in Scheme 1. 4-*n*-Alkylbenzenes **5** were prepared by Tamao–Kumada reaction.<sup>13</sup> All the complexes except for C<sub>1</sub>–Ni and C<sub>2</sub>–Ni were recrystallized from ethyl acetate. The recrystallization solvent for C<sub>1</sub>–Ni and C<sub>2</sub>–Ni was dioxane. These C<sub>*n*</sub>–Ni complexes obtained from recrystallization are black for *n* = 1–5, dark green for *n* = 6 and green for *n* = 7–12, as summarized in Table 1.

**Table 1** The crystalline shapes<sup>a</sup> and colors obtained from recrystallization for the complexes C<sub>n</sub>-Ni and C<sub>n</sub>O-Ni

<i>n</i>	C <sub>n</sub> -Ni	<i>n</i>	C <sub>n</sub> O-Ni
1	Black needles	1	Black needles
2	Black needles	2	Black needles
3	Black needles	3	Black needles
4	Black needles	4	Black needles
5	Black needles (K <sub>1</sub> )	5	Black needles (K <sub>1</sub> )
6	Dark green needles	6	Dark brown needles (K <sub>1</sub> )
7	Green needles	7	Brown needles (K <sub>1</sub> )
8	Green powder (K <sub>1</sub> )	8	Brown needles (K <sub>1</sub> )
9	Green powder (K <sub>1</sub> )	9	Brown needles (K <sub>2</sub> )
10	Green powder (K <sub>1</sub> )	10	Brown needles (K <sub>1</sub> )
11	Green powder (K <sub>1</sub> )	11	Brown needles (K <sub>1</sub> ) + Plates(K <sub>2</sub> )
12	Green powder (K <sub>1</sub> )	12	Brown needles (K <sub>2</sub> )
		14	Brown needles (K <sub>2</sub> )
		16	Brown needles (K <sub>2</sub> )
		18	Brown needles (K <sub>3</sub> )

<sup>a</sup>All the complexes except for C<sub>1</sub>-Ni and C<sub>2</sub>-Ni were recrystallized from ethyl acetate. The recrystallization solvent for C<sub>1</sub>-Ni and C<sub>2</sub>-Ni was dioxane.

**Synthesis C.** A novel synthetic route to the C<sub>n</sub>O-Ni complexes for *n* = 14, 16 and 18 is shown in Scheme 3. These C<sub>n</sub>O-Ni complexes recrystallized from ethyl acetate are **brown**, as summarized in Table 1. The detailed procedures are described only for the representative complex C<sub>14</sub>O-Ni in the following:

**4,4'-Bis(tetradecyloxy)benzil 4.** In an atmosphere of dry nitrogen, anhydrous potassium carbonate, 0.74 g (5.4 mmol), and *n*-tetradecyl bromide, 1.5 g (5.4 mmol), were added to a solution of 4,4'-dihydroxybenzil, 0.52 g (2.2 mmol), in 20 ml of *N,N*-dimethylacetamide and the mixture was stirred for 17 hours at 90 °C. The reaction mixture was extracted with chloroform. The organic layer was washed with water, dried over sodium sulfate and the solvent was evaporated. The purification was carried out by recrystallization from ethyl acetate to give 1.0 g of white crystals **4**. Yield 73%; mp 73.7 °C; IR (KBr pellet, cm<sup>-1</sup>): 2940, 2850, 1660, 1600, 1260. <sup>1</sup>H-NMR (CDCl<sub>3</sub>, TMS): δ/ppm = 0.90(m, 6H, -CH<sub>3</sub>), 1.30(m, 48H, -(CH<sub>2</sub>)<sub>2</sub>-), 4.02(t, *J* = 6.3 Hz, 4H, CH<sub>2</sub>), 6.89(d, *J* = 7.8 Hz, 4H, arom. H), 7.87(d, *J* = 7.8 Hz, 4H, arom.-H).

**Bis[1,2-bis(4-*n*-tetradecyloxyphenyl)ethane-1,2-dithiolene]-nickel I.** A mixture of 1.0 g (1.6 mmol) of 4,4'-bis(tetradecyloxy)benzil **4**, 1.4 g (3.2 mmol) of phosphorus pentasulfide, and 40 ml of dioxane was refluxed for 5 hours. The hot reaction mixture was filtered to remove the unreacted phosphorus pentasulfide and washed with a small portion of hot dioxane. And a solution of nickel(II) dichloride hexahydrate, 0.19 g (0.79 mmol), in 8 ml of ethanol was added to the filtrate and the reaction mixture was refluxed for 2 hours. After it had been cooled by immersion in an ice-water bath, a brown powder was formed and was collected by filtration to give the crude complex **1**. Purification was performed by recrystallization from ethyl acetate to afford 0.62 g of brown needle like crystals. Yield 57%; cp 163.2 °C; IR (KBr pellet, cm<sup>-1</sup>): 2930, 2860, 1600, 1510, 1470, 1360, 1300, 1250, 1170, 1140, 880; <sup>1</sup>H-NMR (CDCl<sub>3</sub>, TMS) δ/ppm = 0.88(t, *J* = 4 Hz, 12H, -CH<sub>3</sub>), 1.26–1.49(m, 96H, -(CH<sub>2</sub>)<sub>2</sub>-), 3.9(t, *J* = 6 Hz, 8H, -OCH<sub>2</sub>-), 6.50(d, *J* = 4.2 Hz, 8H, arom.-H), 6.96(d, *J* = 4.2 Hz, 8H, arom.-H); Anal. Found (Calcd. for C<sub>84</sub>H<sub>132</sub>O<sub>4</sub>S<sub>4</sub>Ni): C 72.36% (72.43%), H 9.54% (9.55%).

## 2.2 Measurements

The complexes **1** and **2** were identified by elemental analysis using a Perkin-Elmer Elemental Analyzer 240B. The phase transition behaviors of **1** and **2** were observed with a polarizing

microscope, Olympus BH-2, equipped with a heating plate controlled by a thermoregulator, Mettler FP80 and 82, and measured with differential scanning calorimeters, a Rigaku Thermoflex TG-DSC. To establish the mesophases, powder X-ray patterns were measured with Cu-Kα radiation using a Rigaku Geigerflex equipped with a hand-made heating plate controlled by thermoregulator.<sup>15</sup> Reduction potentials of these complexes were measured with cyclic voltammetry, Yanagimoto Polarographic Analyzer P-1100, in methylene chloride solutions containing 0.1 M tetrabutylammonium perchlorate as supporting electrolyte. The measurements were made at glassy-carbon working electrode vs. a saturated calomel electrode (SCE); sweep rates 10 mV sec<sup>-1</sup>.

## 3. Results and discussion

### 3.1 Synthesis

The problem of the synthetic routes in Schemes 1 and 2 is that the length of the chains must be determined in the early stage. Moreover, disposal of the unreacted selenium dioxide after the oxidation reaction is very difficult and expensive. Therefore, we have synthesized the C<sub>n</sub>O-Ni complexes for *n* = 14, 16, and 18 by a new synthetic route as shown in Scheme 3. The benzil derivatives **4** were synthesized from 4-methoxybenzaldehyde by the method of Wenz.<sup>16</sup> This synthetic route is advantageous for the synthesis of a series of the homologues with different length of the lateral chains, because the alkylation in the late stage permits us to use a common precursor, **11**, for all the complexes.

**Table 2** Phase transition temperatures (*T*) and enthalpy changes ( $\Delta H$ ) of C<sub>n</sub>-Ni

<i>n</i>	Phase	$T/^\circ\text{C}$ [ $\Delta H/\text{kJ mol}^{-1}$ ]	Phase <sup>a</sup>
1	K	322	I.L.(decomp.)
		→	
2	K	290	I.L.(decomp.)
		→	
3	K	270	I.L.(decomp.)
		→	
4	K	228	I.L.(decomp.)
		→	
5	K <sub>1</sub>	204[2.1] → 210[46.4]	I.L.
		←	
6	K	201[69.0]	I.L.
		←	
7	K	187[60.7]	I.L.
		←	
8	K <sub>1</sub>	149[5.9] → 182[61.5]	I.L.
		←	
9	K <sub>1</sub>	126[8.8] → 175[61.1]	I.L.
		←	
10	K <sub>1</sub>	128[11.7] → 172[65.7]	I.L.
		←	
11	K <sub>1</sub>	135[13.4] → 166[72.0]	I.L.
		←	
12	K <sub>1</sub>	134[19.2] → 162[70.7]	I.L.
		←	

<sup>a</sup>Phase nomenclature: K = crystal and I.L. = isotropic liquid.

**Table 3** Phase transition temperatures ( $T$ ) and enthalpy changes ( $\Delta H$ ) of the  $C_n$ -Ni ( $n = [1-18]$ ) complexes

$n$	Phase	$T/^\circ\text{C}$ [ $\Delta H/\text{kJ mol}^{-1}$ ]	Phase <sup>a</sup>	$n$	Phase	$T/^\circ\text{C}$ [ $\Delta H/\text{kJ mol}^{-1}$ ]	Phase <sup>a</sup>
1	K	324	I.L. (decomp.)	10	$K_1$ (b)	88.0[16.3]	$K_2$ (b)
2	K	316	I.L. (decomp.)	10	$K_1$ (b)	95 ~ 105[17.2]	$D_1$ (b)
3	K	289	I.L. (decomp.)	10	$K_1$ (b)	114.9[30.1]	$K_3$ (g)
4	K	249	I.L. (decomp.)	10	$K_1$ (b)	125.6[22.2]	$D_2$ (g)
5	$K_2$	194.6[12.1]	$K_3$	10	$K_1$ (b)	183.2[58.2]	I.L. (g)
5	$K_1$	178.1[12.6]	I.L.	11	$K_2$ (b)	89.2[43.1]	$D_1$ (b)
5	$K_1$	131.2	I.L.	11	$K_2$ (b)	107 ~ 122[ca. 6.7]	$D_2$ (g)
5	$K_2$	182.1[2.5]	I.L.	11	$K_1$ (g)	76.3[21.8]	$K_1$ (g)
6	$K_4$ (g)	108.5[3.3]	$K_5$ (g)	11	$K_1$ (g)	177.0[60.7]	I.L. (g)
6	$K_1$ (b)	96 ~ 102[ca. 6.7]	$K_2$ (b)	12	$K_2$ (b)	73.0[108.8]	$D_1$ (b)
6	$K_1$ (b)	117 ~ 136[12.1]	$K_3$ (g)	12	$K_2$ (b)	122 ~ 131[ca. 18]	$D_2$ (g)
6	$K_1$ (b)	117 ~ 122[ca. 13.0]	$K_4$ (g)	12	$K_1$ (g)	56.2[31.0]	$K_1$ (g)
7	$K_2$ (g)	182.1[2.5]	$K_3$ (g)	14	$K_2$ (b)	98.7[28.0]	$D_1$ (b)
7	$K_1$ (b)	117 ~ 136[12.1]	$K_4$ (g)	14	$K_2$ (b)	163.2[45.2]	$D_2$ (g)
7	$K_1$ (b)	117 ~ 122[ca. 13.0]	$K_5$ (g)	16	$K_2$ (b)	101.6[35.6]	$D_1$ (b)
7	$K_2$ (g)	108.5[3.3]	$K_3$ (g)	16	$K_2$ (b)	111 ~ 118[ca. 13]	$D_2$ (g)
7	$K_1$ (b)	96 ~ 102[ca. 6.7]	$K_4$ (g)	16	$K_1$ (g)	74.9[32.6]	$K_1$ (g)
7	$K_1$ (b)	117 ~ 122[ca. 13.0]	$K_5$ (g)	16	$K_1$ (g)	156.6[55.2]	I.L. (g)
8	$K_2$ (g)	79.1[18.0]	$K_3$ (g)	18	$K_3$ (b)	87.9[40.6]	$D_1$ (b)
8	$K_2$ (g)	96 ~ 99[ca. 2.5]	$K_4$ (g)	18	$K_3$ (b)	149.8[55.6]	$D_2$ (g)
8	$K_2$ (g)	117 ~ 122[ca. 13.0]	$K_5$ (g)	18	$K_1$ (g)	73.2[24.7]	$K_1$ (g)
8	$K_2$ (g)	109.0[25.9]	$K_4$ (g)	18	$K_1$ (g)	103 ~ 111[ca. 7.1]	$D_2$ (g)
9	$K_2$ (b)	130.2[33.9]	D (g)	18	$K_1$ (g)	149.8[55.6]	I.L. (g)
9	$K_2$ (b)	189.0[64.0]	I.L. (g)	18	$K_1$ (g)	177.0[60.7]	I.L. (g)

<sup>a</sup>Phase nomenclature: K = crystal, D = columnar mesophase, and I.L. = isotropic liquid. (b) and (g) are the color of K, D, and I.L.: (b) = brown, (g) = green.

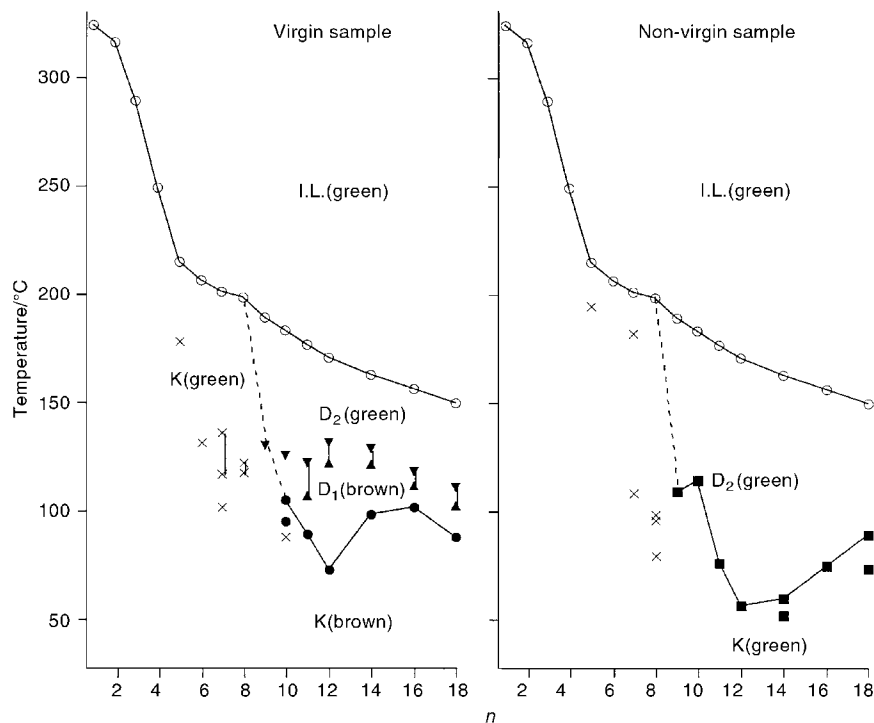


**Fig. 1** Phase transition temperature *versus* number of the carbon atoms in the alkoxy chain ( $n$ ). Open circles: clearing points. Filled circles and squares: melting points of brown crystals and green crystals, respectively. Triangles: phase transitions from brown D<sub>1</sub> to green D<sub>2</sub>. Crosses: crystal-crystal phase transition.

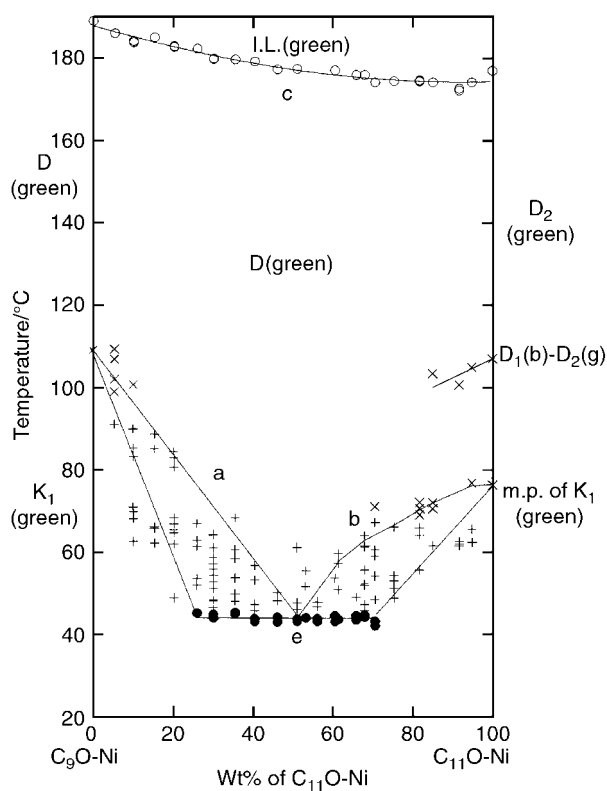
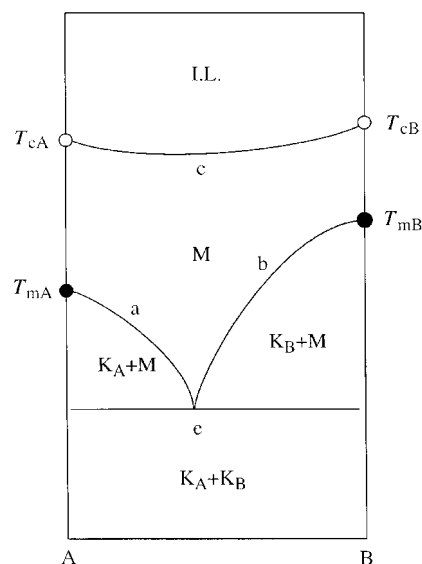


**Fig. 2** Miscibility diagram between C<sub>9</sub>O-Ni and C<sub>11</sub>O-Ni. Points in the miscibility diagram were onset temperatures observed in the DSC measurements as the peaks or shoulders. The open and filled circles could be observed as clear and big peaks, but most of the crosses were observed as complicated small peaks and shoulders. Curves a and b: freezing depression curves. Curve c: clearing point curve. Point e: eutectic point.

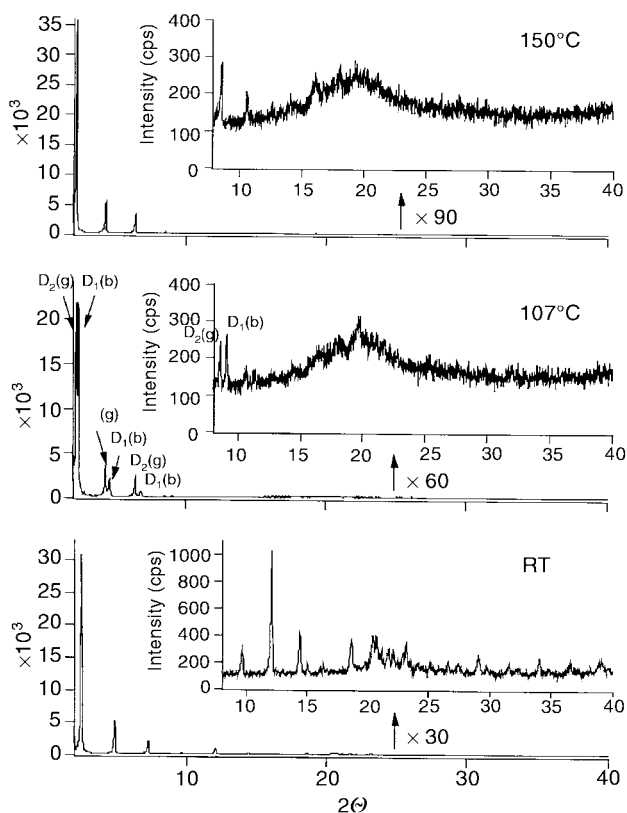
### 3.2 Thermal behavior of C<sub>*n*</sub>-Ni ( $n=1-12$ )

Table 2 summarizes the phase transition temperatures and the phase transition enthalpy changes ( $\Delta H$ ) which were determined by the DSC measurements and polarizing microscopic observations. None of the C<sub>*n*</sub>-Ni complexes show a mesophase.

It is noteworthy that these C<sub>*n*</sub>-Ni complexes obtained from recrystallization are **green** for  $n=7-12$ , whereas the C<sub>*n*</sub>O-Ni complexes recrystallized from ethyl acetate are **brown** for  $n=7-18$ , as summarized in Table 1. This is very suggestive of a color change from **brown** D<sub>1</sub> mesophase to **green** D<sub>2</sub> mesophase in C<sub>*n*</sub>O-Ni complexes for  $n \geq 10$ , as will be described in the latter part of this paper.



**Fig. 3** A schematic miscibility diagram between two pure compounds, A and B. Filled and open circles represent melting points ( $T_{mA}$  and  $T_{mB}$ ) and clearing points ( $T_{cA}$  and  $T_{cB}$ ) of the pure compounds, respectively. Curves a and b: freezing depression curves. Curve c: clearing point curve. Point e: eutectic point.



**Fig. 4** Temperature-dependent X-ray diffraction patterns of  $C_{16}O-Ni$  at rt, 107 and  $150^\circ C$ . The peaks denoted  $D_1(b)$  and  $D_2(g)$  in this figure are reflections due to the brown  $D_1$  and green  $D_2$  phases, respectively.

### 3.3 Thermal behavior of $C_nO-Ni$ ( $n=1-18$ )

Table 3 summarizes the phase transition temperatures and the phase transition enthalpy changes ( $\Delta H$ ). The  $C_nO-Ni$  complexes for  $n=1-4$  were black needle-like crystals and the crystals directly melt into a green isotropic liquid (I.L.) with rapid decomposition. The  $C_nO-Ni$  complexes for  $n=5-8$  show not a mesophase but crystal-crystal phase transitions.  $C_9O-Ni$  shows a green mesophase, and each of the complexes for  $n \geq 10$  shows two differently colored mesophases. The results of the polarizing microscopic observation are described for the representative  $C_{12}O-Ni$  complex in the following.

When the virgin sample of the brown  $K_2$  crystals was heated, it melted into a brown  $D_1$  mesophase at  $73.0^\circ C$ . On further heating, a slow transition from the brown  $D_1$  phase to a green  $D_2$  phase could be noticed at around  $125^\circ C$ . The green  $D_2$  phase cleared into a green I.L. at  $170.8^\circ C$ . On cooling down to around  $167^\circ C$ , the green I.L. changed into green smooth plates surrounded by lustrous rings. On further cooling, the green plates and rings were cracked and changed into green  $K_1$  crystals at around  $56^\circ C$ . When the green  $K_1$  phase was heated again, it melted into the green  $D_2$  phase at  $56.2^\circ C$  and then the green  $D_2$  phase cleared into the green I.L. at  $170.8^\circ C$ . Thus, for the non-virgin sample, neither the brown  $K_2$  nor  $D_1$  phases appeared. Hence, only virgin sample of the complex can give the brown  $K_2$  crystalline phase and the brown  $D_1$  mesophase. However, it should be emphasized that the brown virgin form could return on recrystallization of the green non-virgin sample from the solvent, ethyl acetate.

In DSC measurements, the peak due to the transition from brown  $D_1$  phase to green  $D_2$  phase showed a heating rate dependence. The faster the heating rate was, the higher the transition temperature became ( $122-131^\circ C$ ). This phenomenon was observed for each of the  $C_nO-Ni$  complexes for  $n \geq 10$ . Thus, the color change from  $D_1(b)$  to  $D_2(g)$  is significantly slow. For  $n=7-8$ , the color change could be

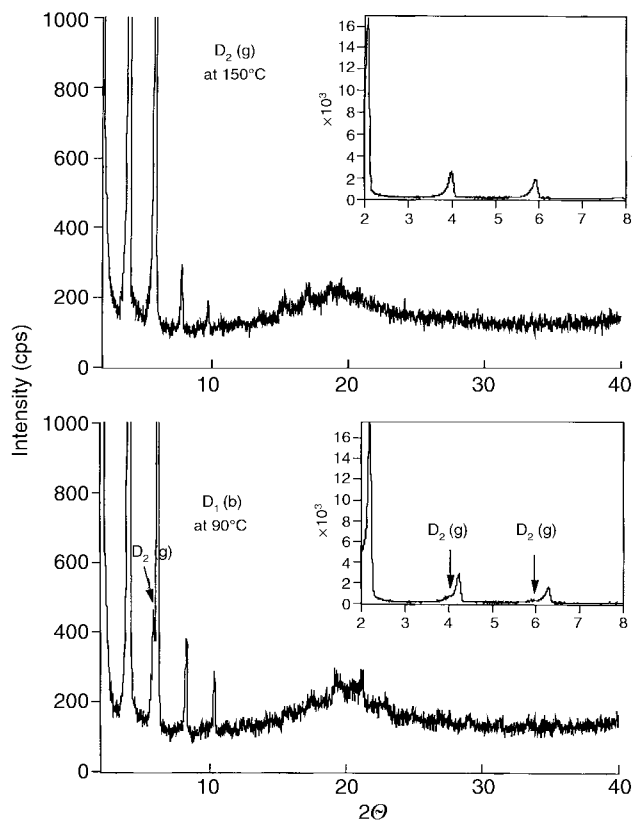


**Fig. 5** Temperature-dependent X-ray diffraction patterns of  $C_{18}O-Ni$  at 90 and  $150^\circ C$ . The peaks denoted  $D_1(b)$  and  $D_2(g)$  in this figure are reflections due to the brown  $D_1$  and green  $D_2$  phases, respectively.

observed for a transition from brown crystal to green crystal. For  $n=9$ , it was observed for a transition from brown crystal  $K_2$  to green mesophase  $D(g)$ .

In Fig. 1, phase transition temperatures of the virgin samples and the non-virgin samples are separately plotted against the carbon number ( $n$ ) in the alkoxy-side-chain. As can be seen from this figure, each of the virgin samples  $n \geq 10$  gives both brown and green mesophases, whereas the non-virgin sample does not show the brown mesophase but only the green mesophase.

Although we reported the  $C_{11}O-Ni$  complex gives only one mesophase in our previous papers,<sup>9,10</sup> the present detailed reinvestigation revealed that it has two differently colored mesophases like the other complexes for  $n=10, 12-18$ . Therefore, we correct the phase transition sequence of the  $C_{11}O-Ni$  complex as shown in Table 2. Although Veber *et al.*

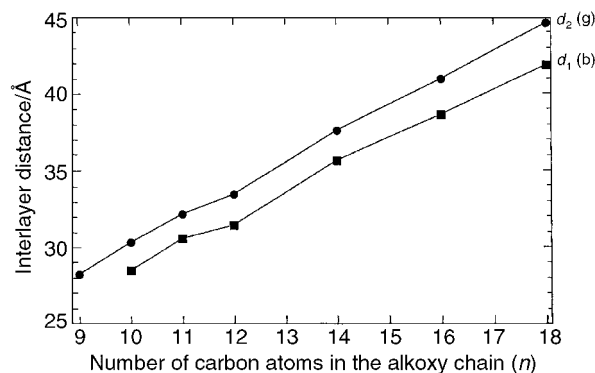


**Fig. 6** Interlayer distance ( $\text{\AA}$ ) versus number of carbon atoms in the alkoxy chain ( $n$ ).  $d_1(b)$  and  $d_2(g)$  represent the interlayer distances due to the brown  $D_1$  and green  $D_2$  phases, respectively.

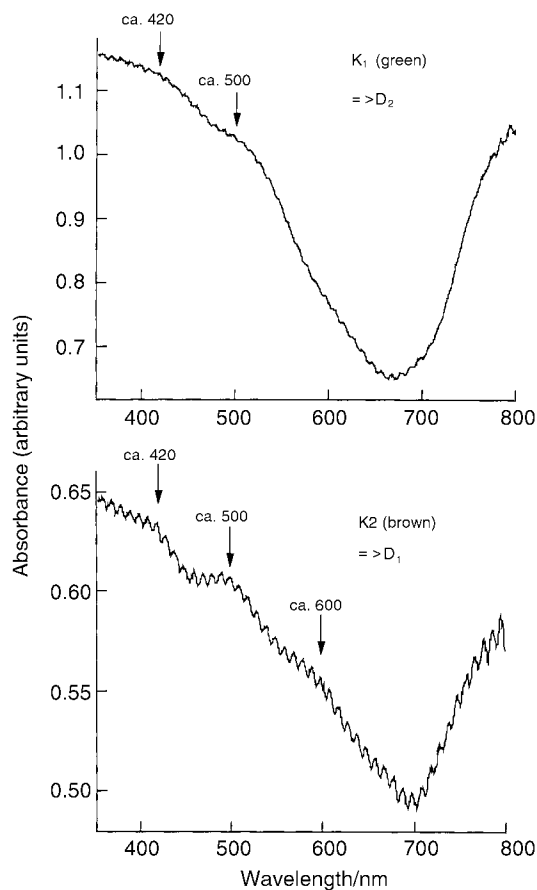


**Fig. 7** Solid absorption spectra of the green K<sub>1</sub> and brown K<sub>2</sub> phases of C<sub>12</sub>O–Ni. Fine powders of these solids were dispersed in transparent silicone oil and placed between two P-102 glass plates. This dispersion avoided the dissolution of these solids into their green solution, so that the brown colored K<sub>2</sub> crystals remained without changing the color.

reported only one mesophase for the C<sub>12</sub>O–Ni complex,<sup>8</sup> it has two mesophases of brown D<sub>1</sub> and green D<sub>2</sub> as described above.

### 3.4 Miscibility diagram between C<sub>11</sub>O–Ni and C<sub>9</sub>O–Ni

Previously, we carried out miscibility tests between the C<sub>11</sub>O–Ni and C<sub>9</sub>O–Ni complexes<sup>9,10</sup> in order to establish mesomorphism of these C<sub>n</sub>O–Ni complexes. However, at that time we noticed only a green mesophase for the C<sub>11</sub>O–Ni complex. Since we found another brown mesophase for this complex in this work, we reexamined the miscibility between the C<sub>11</sub>O–Ni and C<sub>9</sub>O–Ni complexes. As a result, a miscibility diagram was obtained as shown in Fig. 2. These tests were carried out for the non-virgin samples. Although the non-virgin sample cannot give the phase transitions from brown D<sub>1</sub> to green D<sub>2</sub> as

**Table 4** Main features of the experimental electronic spectra for the C<sub>12</sub>O–Ni and Ni(S<sub>2</sub>C<sub>2</sub>H<sub>2</sub>)<sub>2</sub> complexes

C <sub>12</sub> O–Ni		Ni(S <sub>2</sub> C <sub>2</sub> H <sub>2</sub> ) <sub>2</sub> <sup>a</sup>	
Green K <sub>1</sub> solid film λ <sub>max</sub> /nm	Brown K <sub>2</sub> solid film λ <sub>max</sub> /nm	In CHCl <sub>3</sub> λ <sub>max</sub> /nm	In <i>n</i> -hexane λ <sub>max</sub> /nm
			860
			719
			550 B <sub>1u</sub> (z)
ca. 500	ca. 600	625	444
ca. 420	ca. 500	468	370 B <sub>2u</sub> (y)
	ca. 420	337	290
		302	270
		280	210

<sup>a</sup>Ref. 19.

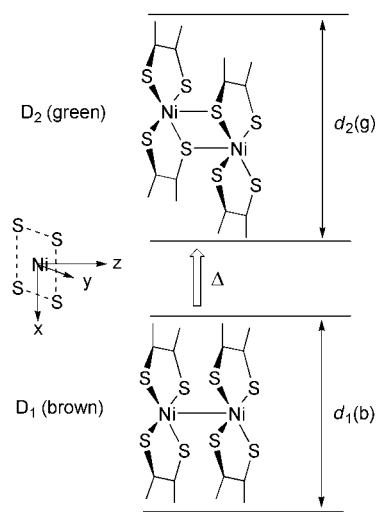


**Fig. 8** Tentative transformation from the nickel–nickel bonded dimer D<sub>1</sub> mesophase to the nickel–sulfur bonded dimer D<sub>2</sub> mesophase.

mentioned above, the non-virgin sample of the C<sub>11</sub>O–Ni complex gave a short curve corresponding to the transition from the brown D<sub>1</sub> phase to green D<sub>2</sub>. The curve obviously starts from the transition temperature from the brown D<sub>1</sub> phase to green D<sub>2</sub> at 107 °C of the C<sub>11</sub>O–Ni complex and disappears at ca. 80 wt%. The reason for the appearance of this curve is not clear at the present time.

As can be seen from this figure, an area of green D phase exists over two freezing depression curves (a and b) and under a clearing point curve (c). Generally, a pure compound can be thermodynamically divided into two phases between the crystalline phase (K) and liquid (L) at the melting point (T<sub>m</sub>), as follows:



Hence, the mp (T<sub>m</sub>) is the boundary between K and L. For a mixture of two components, A and B, as schematically illustrated in Fig. 3, both of the freezing point depression curves (a and b) start from their melting points of the pure A and B components (T<sub>mA</sub>, T<sub>mB</sub>). Therefore, these freezing depression curves, a and b, also show the boundary between crystalline phase and liquid. Hence, the area (M) over these two freezing depression curves (a and b) with a eutectic point (e) must have the characteristics of a liquid, thermodynamically. Generally, liquid crystalline phases of a mixture of two compounds can be seen in areas over two freezing depression curves (a and b) with a eutectic point (e) and under a clearing point curve (c). As can be seen from Fig. 2, the area denoted as D (green) phase could be observed over two freezing depression curves (a and b) with the eutectic point (e: 51 wt% 43.8 °C) and under the clearing point curve (c). Therefore, we could judge that this area of D (green) thermodynamically shows a mesophase.

### 3.5 Temperature-dependent X-ray diffraction studies on the C<sub>n</sub>O–Ni complexes

Fig. 4 shows X-ray diffraction patterns of C<sub>16</sub>O–Ni at rt, 107 and 150 °C. The pattern at rt shows many fine sharp reflections, which is typical for crystalline phases. The pattern at 107 °C show a halo at around 2θ=20, which corresponds to the molten alkoxy chains. In the low angle region, two sets of periodic reflections corresponding to two lamellar structures could be observed, but the longer- and shorter-spacing of reflections became bigger and smaller, respectively, with time, holding at 107 °C. This gradual change could be detected over

**Table 5** The reduction potential of the complexes,  $C_n$ -Ni and  $C_n$ O-Ni

$n$	$E_{1/2}^a$ of $C_n$ -Ni	Liquid crystallinity
$0^b$	0.03	Non-mesogen
1	-0.01	
2	-0.02	
3	-0.01	
4	-0.01	
5	-0.01	
6	-0.03	
7	-0.03	
8	-0.03	
9	-0.03	
10	-0.03	
11	-0.03	
12	-0.02	

$n$	$E_{1/2}^a$ of $C_n$ O-Ni	Liquid crystallinity
1	-0.05	Non-mesogen
2	-0.06	
3	-0.06	
4	-0.06	
5	-0.05	
6	-0.06	
7	-0.05	
8	-0.05	
9	-0.06	Mesogen
10	-0.06	
11	-0.07	
12	-0.06	

<sup>a</sup>Volts vs. SCE in  $CH_2Cl_2$ . <sup>b</sup>Bis(diphenyldithiolene)nickel.

one hour. These longer-spacings of reflections correspond to reflections of the higher temperature mesophase  $D_2$ . For the DSC measurements at  $10^\circ C \text{ min}^{-1}$  heating rate, the transition from  $D_1$  to  $D_2$  could be observed as a broad endothermic peak at  $111$ – $118^\circ C$ . However, this X-ray diffraction pattern was recorded, holding the temperature at  $107^\circ C$ . This means that the transition is so slow that it was detected at higher temperature for the short-time DSC measurements, compared with the long-hour X-ray diffraction measurements. Hence, it is obvious that the brown  $D_1$  mesophase is not so stable even under the  $D_1$ – $D_2$  phase transition temperature observed by DSC. This instability made it very difficult to record an X-ray diffraction pattern of the pure brown  $D_1$  mesophase, but the  $D_1$  phase could be assigned as a lamellar type of mesophase. The pattern at  $150^\circ C$  showed a set of periodic reflections, (001), (002), (003), (004) and (005), at low angle region corresponding to a lamellar structure, and a very broad halo due to the molten alkoxy chains in the medium angle region. Hence, this  $D_2$  phase could also be assigned as a lamellar type of mesophase. The difference between these two lamellar mesophases is color: the  $D_1$  and  $D_2$  mesophases are brown and green, respectively.

Fig. 5 shows X-ray diffraction patterns of  $C_{18}O$ -Ni at  $90$  and  $150^\circ C$ , corresponding to the brown  $D_1$  and green  $D_2$  mesophases, respectively. Even at  $90^\circ C$ , which is low enough from the  $D_1$  (b)– $D_2$  (g) phase transition temperature ( $103$ – $111^\circ C$ ) observed by DSC, the X-diffraction pattern still contains some reflections due to the  $D_2$  (g) mesophase (Fig. 5). From these X-ray patterns, both the brown  $D_1$  and green  $D_2$  mesophases could be assigned as lamellar types of mesophases.

Generally, disk-like molecules containing more than six side-chains pile up one-dimensionally to give columnar mesophases. On the other hand, four-chain-substituted disk-like molecules tend to show discotic lamellar mesophases. Although many columnar liquid crystalline compounds have been reported, very few discotic lamellar liquid crystals have been reported. Only four long chain-substituted disk-like metal complexes show discotic lamellar mesophases in most cases.<sup>17</sup> The present

complexes consist of a disk-like core and four peripheral chains. Hence, we concluded that both the  $D_1$  and  $D_2$  phases are discotic lamellar mesophases ( $D_L$ ). The brown  $D_1$  mesophase did not give a natural texture from the green I.L., whereas the green  $D_2$  mesophase gave a natural plane texture surrounded by a lustrous ring as reported previously.<sup>10</sup> This texture resembled very well the texture of the discotic lamellar mesophase  $D_1$  in  $C_8$ -Cu(II)<sup>18</sup> which had been well established as  $D_{L2}$  by miscibility phase diagram and X-ray diffraction studies.<sup>19</sup> These facts also support our present conclusion. It is very interesting that the complexes which consist of the same disk-like core and eight peripheral chains show a hexagonal columnar mesophase ( $Col_h$ ), as previously reported.<sup>20</sup>

The layer distances of these brown  $D_1$  and green  $D_2$  mesophases [ $d_1$  (b),  $d_2$  (g)] are plotted against number of the carbon atoms in the alkoxy chain ( $n$ ), in Fig. 6. As can be seen from this figure, the  $d_2$  (g) distance is about  $2 \text{ \AA}$  longer than the  $d_1$  (b) distance for all the complexes.

### 3.6 Thermochromism of the $C_n$ O-Ni complexes

The  $C_n$ O-Ni complexes for  $7 \geq n$  show a color change from brown to green for their virgin samples. For  $10 \geq n$ , the transition from the  $D_1$  phase to the  $D_2$  phase is accompanied by a color change from brown to green, as described above. In order to establish this color change for  $C_{12}O$ -Ni, we carried out measurements of the solid absorption spectra of the visible region for the brown  $K_2$  crystalline phase of the virgin sample and the green  $K_1$  crystalline phase of the non-virgin sample. These solid fine powder samples were dispersed in transparent silicone oil and placed between two glass plates (Glass techno, P-102 glass) which are transparent at  $2100$ – $300 \text{ nm}$ .

As shown in Fig. 7, the spectrum of the brown  $K_2$  crystalline phase gave three peaks at *ca.*  $420$ , *ca.*  $500$ , and *ca.*  $600 \text{ nm}$ . On the other hand, that of the green  $K_1$  crystalline phase gave two peaks at *ca.*  $420$  and *ca.*  $500 \text{ nm}$ . Thus, the color change from brown to green originates from the lack of the peak at *ca.*  $600 \text{ nm}$ . It can be thought that these spectra of the brown  $K_2$  and green  $K_1$  crystalline phases correspond to those of the brown  $D_1$  and green  $D_2$  mesophases, respectively. It was revealed from X-ray analysis that each of the  $D_1$  and  $D_2$  mesophases is a  $D_L$  mesophase. Since the spectral difference between the  $D_1$  and  $D_2$  mesophases is regarded as the same as that between the  $K_2$  and  $K_1$  crystalline phases, the transition from the brown  $D_1$  phase to the green  $D_2$  phase corresponds to the lack of the peak at *ca.*  $600 \text{ nm}$ .

These peaks were assigned by using electronic spectral analysis for the core complex, bis(ethylene-1,2-dithiolato)-nickel,  $Ni(S_2C_2H_2)_2$ , reported by Herman *et al.*<sup>21</sup> In Table 4 are collected the absorption spectral data of the green  $K_1$  crystalline phase, the brown  $K_2$  crystalline phase, and the chloroform solution (green) of the  $C_{12}O$ -Ni complex, and that of the *n*-hexane solution of  $Ni(S_2C_2H_2)_2$  reported by Herman *et al.* The peaks at  $550$  and  $370 \text{ nm}$  for  $Ni(S_2C_2H_2)_2$  in *n*-hexane have been assigned to  $B_{1u}$  and  $B_{2u}$  symmetry, respectively. The  $B_{1u}$  symmetry contains  $L\pi \rightarrow (L\sigma^* + 0.21dz^2 - 0.84Ni \text{ s})$  transition, which is the transition in the *z*-axis direction and suggests the existence of the Ni-Ni bond. On the other hand, the  $B_{2u}$  symmetry contains  $L\pi \rightarrow L\pi^*$  transition in the *y*-axis direction. These peaks at  $550$  and  $370 \text{ nm}$  of the core complex correspond to *ca.*  $600$  and *ca.*  $420 \text{ nm}$  peaks of the solid absorption spectra of the present  $C_{12}O$ -Ni complex. Therefore, the phase transition from the brown  $D_1$  phase to the green  $D_2$  phase is accompanied by a lack of the peak at *ca.*  $600 \text{ nm}$ , which suggests that the intermolecular Ni-Ni bonds in the *z*-axis direction are broken or weakened. The tentative molecular models in these two  $D_L$  mesophases are proposed as shown in Fig. 8. In the brown  $D_1$  phase, two molecules form a dimer through the Ni-Ni bond between them. When it is heated, the Ni-Ni bond is gradually broken and a new Ni-S bond between



these two molecules slowly forms instead because the Ni–Ni bond is at a higher energy level than a Ni–S bond, that is, the Ni–S bond is more stable than the Ni–Ni bond. Hence, two molecules slip over each other.<sup>22</sup> As shown in Fig. 8, the layer distance of the green D<sub>2</sub> phase (*d*<sub>2</sub> (g)) should be longer than that of the brown D<sub>1</sub> phase (*d*<sub>1</sub> (b)). As can be seen from Fig. 6, the *d*<sub>2</sub> (g) distance is actually longer than the *d*<sub>1</sub> (b) distance for all the complexes for *n* ≥ 10.

Thus, the thermochromism (brown→green) is attributable to the slow transformation from the Ni–Ni bonded dimers to the Ni–S bonded dimers.

### 3.7 Electrochemistry

The half-wave potentials *E*<sub>1/2</sub> for the first reduction of these complexes, C<sub>*n*</sub>–Ni (*n* = 1–12) and C<sub>*n*</sub>O–Ni (*n* = 1–12), are listed in Table 5 with their liquid crystallinity in the right-hand column. In this table, *n* shows the number of the carbon atoms in peripheral chains and *n* = 0 corresponds to the core complex, bis(diphenyldithiolene)nickel. From this table, it is apparent that the reduction potentials of these complexes are nearly constant irrespective of the alkyl or alkoxy chain length. The values, –0.01 to –0.03 vs. SCE, observed for C<sub>*n*</sub>–Ni (*n* = 1–12) are somewhat less positive than that of the core complex (+0.03 V vs. SCE), whereas they are more positive than those of the analogous complexes, C<sub>*n*</sub>O–Ni. The values, –0.05 to –0.07 V vs. SCE, observed for C<sub>*n*</sub>O–Ni (*n* = 1–12) are much less positive than that of the core complex. Thus, the reduction potentials mainly depend on the types of the substituents. It is attributable to the more electron donating property of the alkoxy substituents than that of the alkyl substituents. From Table 5, we can derive a very interesting relationship between the mesomorphic property and reduction potential for changing the alkoxy chain length. The mesomorphic property of the complexes depends on the alkoxy chain length, whereas the reduction potential does not. That is to say, we can change the peripheral chain length to obtain the mesomorphic properties without changing the electrochemical properties. This seems to be very useful for the functionalization of mesogenic compounds.

### 4. Conclusion

Two series of C<sub>*n*</sub>–Ni (*n* = 1–12) and C<sub>*n*</sub>O–Ni (*n* = 1–12, 14, 16, 18), have been synthesized. It was established that the C<sub>*n*</sub>O–Ni complexes exhibit two differently colored discotic lamellar (D<sub>L</sub>) mesophases for *n* ≥ 10, and that the thermochromism (brown→green) is attributable to the slow transformation from the Ni–Ni bonded dimers to the Ni–S bonded dimers. The reduction potential of these complexes does not depend on the chain length, whereas the mesomorphic property does.

### Acknowledgements

This work was partially supported by Grant-in Aid for Research (12129205) by the Ministry of Education, Science, Sports and Culture of Japan.

### References

- 1 Part 30: K. Hatsusaka, K. Ohta, I. Yamamoto and H. Shirai, *J. Mater. Chem.*, 2001, **11**, 423.
- 2 A. M. Giroud-Godquin and P. M. Maitlis, *Angew. Chem., Int. Ed. Engl.*, 1991, **30**, 375; K. Ohta and I. Yamamoto, *J. Synth. Org. Chem. Jpn.*, 1991, **49**, 486.
- 3 A. M. Giroud and U. T. Mueller-Westerhoff, *Mol. Cryst. Liq. Cryst.*, 1977, **41**, 11.
- 4 A. M. Giroud and U. T. Mueller-Westerhoff, *Mol. Cryst. Liq. Cryst.*, 1980, **56**, 225.
- 5 U. T. Mueller-Westerhoff, A. Nazzal, R. J. Cox and A. M. Giroud, *Mol. Cryst. Liq. Cryst.*, 1980, **56**, 249.
- 6 U. T. Mueller-Westerhoff, A. Nazzal, R. J. Cox and A. M. Giroud, *J. Chem. Soc., Chem. Commun.*, 1980, 497.
- 7 P. M. Cotrait, J. Gaultier, C. Polycarpe, A. M. Giroud and U. T. Mueller-Westerhoff, *Acta Crystallogr., Sect. C*, 1980, **C39**, 833.
- 8 M. Veber, R. Fugnitto and H. Strzelecka, *Mol. Cryst. Liq. Cryst.*, 1983, **96**, 221.
- 9 K. Ohta, A. Takagi, H. Muroki, I. Yamamoto, K. Matsuzaki, T. Inabe and Y. Maruyama, *J. Chem. Soc., Chem. Commun.*, 1986, 884.
- 10 K. Ohta, A. Takagi, H. Muroki, I. Yamamoto, K. Matsuzaki, T. Inabe and Y. Maruyama, *Mol. Cryst. Liq. Cryst.*, 1987, **147**, 15.
- 11 M. Veber, P. Davidson, C. Jallabert, A. M. Levelut and H. Strzelecka, *Mol. Cryst. Liq. Cryst., Lett.*, 1987, **5**, 1.
- 12 A. Takagi, MSc Thesis, Shinshu University, Ueda, 1987, Ch. 1, 2
- 13 K. Tamao, K. Sumitani and M. Kumada, *J. Am. Chem. Soc.*, 1972, **94**, 4374; M. Kumada, K. Tamao and K. Sumitani, *Org. Synth.*, 1978, **58**, 127.
- 14 N. Sonoda, Y. Yamamoto, S. Murai and S. Tsutsumi, *Chem. Lett.*, 1972, 229.
- 15 H. Ema, MSc Thesis, Shinshu University, Ueda, 1988, Ch. 7
- 16 G. Wenz, *Makromol. Chem., Rapid Commun.*, 1985, **6**, 577.
- 17 K. Ohta, R. Higashi, M. Ikejima, I. Yamamoto and N. Kobayashi, *J. Mater. Chem.*, 1998, **8**, 1979; and references cited therein.
- 18 K. Ohta, H. Muroki, A. Takagi, I. Yamamoto and K. Matsuzaki, *Mol. Cryst. Liq. Cryst.*, 1986, **135**, 247.
- 19 K. Ohta, H. Muroki, A. Takagi, K. Hatada, H. Ema, I. Yamamoto and K. Matsuzaki, *Mol. Cryst. Liq. Cryst.*, 1986, **140**, 131.
- 20 K. Ohta, Y. Inagaki-Oka, H. Hasebe and I. Yamamoto, *Polyhedron*, 2000, **19**, 276.
- 21 Z. S. Herman, R. F. Kirchner, G. H. Loew, U. T. Mueller-Westerhoff, A. Nazzal and M. C. Zerner, *Inorg. Chem.*, 1982, **21**, 46.
- 22 S. Alvarez, R. Vicente and R. Hoffmann, *J. Am. Chem. Soc.*, 1985, **107**, 6253; I. Okura, N. Kaji, S. Aono, T. Kita and A. Yamada, *Inorg. Chem.*, 1985, **24**, 453.